J Low Temp Phys
DOI 10.1007/s10909-007-9516-5

# Helium Adsorption on Lithium Substrates

**E. Van Cleve · P. Taborek · J.E. Rutledge**

Received: 25 July 2007 / Accepted: 13 September 2007


**Abstract** We have developed a cryogenic pulsed laser deposition (PLD) system to deposit lithium films onto a quartz crystal microbalance (QCM) at 4 K. Adsorption isotherms of $^4$He on lithium were measured in the temperature range between 1.42 K and 2.5 K. The isotherms are qualitatively different from isotherms on strong substrates such as gold and weak substrates such as cesium. There is no evidence of the formation of solid-like layers of helium, and the helium coverage is approximately linear in the pressure over a wide range. By measuring the low coverage slope of the isotherms, the binding energy of helium to lithium was found to be approximately $-13.6$ K. For lithium substrates less than approximately 100 layers thick, the chemical potential at which the superfluid transition was observed was surprisingly sensitive to the details of lithium deposition.

**Keywords** Helium films · Pulsed laser deposition · Superfluidity · Alkali metal

## 1 Introduction

When helium is adsorbed onto a strong heterogenous substrate such as gold, the first 2 or 3 statistical layers are solid-like. The nature of these layers is not yet clear, but the layers are amorphous and do not participate significantly in superflow at high coverages. Superfluidity on strong substrates requires a minimum critical coverage to saturate the solid-like layers, and the superfluid phase which forms at higher coverages flows over these layers and does not interact directly with the strong, short range

This work was supported by NSF grant DMR 0509685.

E. Van Cleve (✉) · P. Taborek · J.E. Rutledge
Department of Physics and Astronomy, University of California, Irvine, California 92697, USA
e-mail: vancleve@uci.edu

part of the substrate potential. There has been considerable theoretical and experimental work directed at understanding the role of the substrate potential on superfluid onset, and on finding material combinations which result in weaker substrates which would minimize or eliminate the solid-like layers [1–5]. One experimental strategy is to preplate strong substrates with low polarizability and/or low density materials such as solid neon or hydrogen. Experiments with solid hydrogen have reduced the critical coverage to approximately 1/2 layer [6–9]. Another strategy is to exploit the theoretically predicted and experimentally verified weak adsorption potentials of the alkali metals [10].While hydrogen is a weak substrate because of its low density, the alkali metals are weak because the repulsive part of the potential has an anomalously long range. Calculations suggest that the binding strength of the adsorption potential is inversely related to the atomic mass of the alkali metal. Experiments show that cesium, which is the heaviest stable alkali metal, appears to be the weakest substrate, with a wetting transition for $^4$He near T = 2.1 K and an accompanying prewetting transition which occurs at higher temperatures [11, 12]. The experimental signature of prewetting is a discontinuity in film thickness as a function of pressure or chemical potential at constant T. The discontinuity marks a first order phase transition in undersaturated films between a thin film (dry) phase, and a thick film (wet) phase. In contrast to cesium, the wetting scenario of $^4$He on rubidium is not yet understood. Two experiments [13, 14] have located a prewetting-like line for $^4$He on rubidium that does not intersect the bulk liquid-vapor phase boundary. Thus these experiments indicated that $^4$He wets rubidium at all temperatures. A third experiment, although unable to locate a wetting or prewetting transition, suggests that the rubidium is not wet by $^4$He at least up to T = 0.3 K [15]. Some theoretical work has been done to address these experimental results [16, 17]. In these weak binding systems, the prewetting-like discontinuity precludes the possibility of continuously varying the coverage at fixed temperature, so it is not possible to study, for example, monolayer superfluidity, because monolayer films are not stable. The lighter alkalis are expected to have stronger adsorption potentials which eliminate the prewetting-like transitions and yield continuous film growth. In particular, lithium is predicted to have an adsorption potential strong enough to guarantee continuous film growth, but weak enough to prevent formation of solid-like layers; in this sense, it is an intermediate strength substrate [1].

The alkali metals are notoriously reactive and difficult to deal with. Cs and Rb can be conveniently thermally evaporated from glass ampules maintained slightly above room temperature while the substrate is held near 4 K. Thermal evaporation of lithium requires substantially higher temperatures, and therefore much higher heat loads to the cryostat and greater risks of outgassing and surface contamination. Several laboratories have successfully used getter type alkali metal dispensers to make films for wetting studies [18]. However alkali metal dispensers require 4.5 to 7 amps of current to operate, and reach temperatures near 1000 K. The resulting radiative heat load is likely to out-gas the walls of our non-UHV compatible sample cell and the low resistance wiring necessary to carry the current is not compatible with the experiments below 1 K that we plan. These problems motivated our development of a low temperature pulsed laser deposition (PLD) system which utilizes a pulsed YAG laser to develop very high temperatures at a localized spot on a target while maintaining the rest of the apparatus at low temperatures. PLD has been used to form a

variety of films [19, 20], including metals, semiconductors, and superconductors onto room temperature targets, but this is the first application of PLD to film deposition at low temperatures that we are aware of. In this paper we describe the design and performance of the cryogenic PLD system as well as adsorption isotherms of $^4$He on lithium substrates. The features of the isotherms are consistent with the predictions of several recent calculations [3, 21]. In particular, $^4$He wets lithium above T = 1.4 K, but there is no evidence of either prewetting or solid-like layer formation. The slopes of the isotherms in the normal phase provide an estimate of the binding energy of helium to lithium, which we find to be approximately $-13.7 \pm 1$ K. The QCM can also be used to detect the standard signatures of the Kosterlitz-Thouless superfluid transition. On lithium films less than approximately 100 layers thick, two distinct KT-like transitions were observed at different values of the vapor pressure, or equivalently, the chemical potential while the temperature was kept constant. Several annealing procedures were tried to make the substrates more homogeneous, but the peculiar two step superfluid transition was a robust feature of the thinner lithium substrates. Lithium substrates in the range of 200 layers thick had only a single superfluid transition.

## 2 Experimental Methods

Our PLD setup consisted of a pulsed Nd:YAG laser and an optical cryostat similar to that described in [22]; the arrangement is shown in Fig. 1. A sample cell which contained the lithium target and the QCM was suspended in a vacuum, and surrounded by a 10 K thermal shield, a 77 K shield, and finally by an external vacuum vessel. The windows in the thermal shields were made of KG-1 IR absorbing glass to minimize heat leaks from room temperature radiation, while the windows on the sample cell were sapphire to avoid the possibility of laser damage. The laser beam propagated perpendicular to the windows and struck the lithium target at an angle of approximately 32°. The material ablated from the target emerges approximately normal to the target (and independent of the laser beam direction) in a cone with an angle of approximately 20°. The QCM on which the films were deposited was 3 cm from the target. A shadow mask ensured that lithium was deposited only on the central electrode region of the QCM. Since the QCM responds to mass on both of its planar surfaces, both surfaces were covered with lithium. This was accomplished by mounting the QCM on a low temperature compatible stepper motor. The rotation stage also served as an evaporation shutter because the QCM could be rotated into a position in which the ablated material hit a beam stop and did not deposit on either side.

The laser light had a wavelength of 532 nm and a fixed pulse width of 10 ns. The pulse repetition rate was fixed at 30 Hz. The energy was adjusted between 50 and 100 mJ/pulse as measured by thermal laser power meter. If the laser beam was directed onto the same spot of the target for more than approximately 100 pulses, a pit was created which noticeably affected the spatial distribution of ablated material. To avoid this problem, a computer controlled mirror with two axes of rotation (H in Fig. 1) was programmed to raster the beam over an area of approximately 1 cm$^2$. The light was focused using a 450 mm focal length plano-convex room temperature lens through the cryostat windows and into an approximately 1 mm diameter spot on the

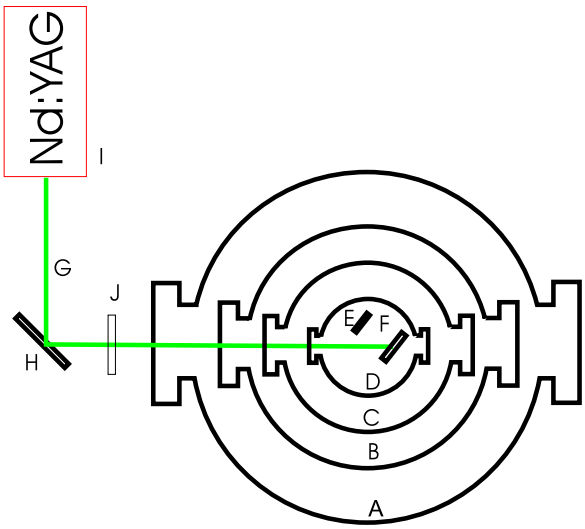


**Fig. 1** (Color online) A diagram of the experimental apparatus. *A* is the outer can. *B* is the nitrogen shield which is in thermal contact with a nitrogen bath. The windows on this shield are KG-1 glass. *C* is the helium shield which is in thermal contact with a helium bath. The glass on this shield is also KG-1. *D* is the cell which is weakly thermally connected to the helium bath. The window on the cell that the laser, *G*, passes through is sapphire. *F* is the lithium target. *E* is the QCM. *H* is the mirror that moves the laser beam around on the target and *I* is the laser itself. *J* is the lens

target. The initial alignment and focusing of the laser was performed with the laser at a low power below the ablation threshold. An LED mounted in the sample cell that would function even at 4 K also helped in the initial alignment.

Preliminary tests to determine the optimal parameters for ablation were performed with the sample cell at room temperature. Target materials that were used in these room temperature studies included copper, silver, gold, lead, carbon, lithium and tungsten. Specular mirror-like films of all of these materials were produced. The background pressure in the cell during the ablation was less than $2 \times 10^{-5}$ Torr. In most cases, the film material was deposited onto the surface of a QCM, which provided a direct determination of the deposition rate. The deposition rate was zero until a threshold power was reached which varied considerably from one target material to the other. Above the threshold power, a plasma ball approximately 5 mm in diameter was visible around the laser spot. As the power was increased above threshold, the deposition rate would initially increase, but as the power was increased further, the deposition rate would plateau and for some materials would eventually decrease.

Because lithium reacts strongly with air, special procedures were required to prepare the target. Lithium was purchased as 1 cm diameter rods packaged under mineral oil. The rods were cut into slices approximately 1 mm thick using a razor blade and then flattened into a disk approximately 2 cm in diameter while under mineral oil. The lithium disks were washed in hexane to clean off the mineral oil and subsequently kept under hexane to prevent the lithium from reacting with air. The final stages of the assembly of the apparatus involved removing the lithium disk from the hexane and transferring it through the air and mounting it in the sample cell, which was then evacuated as quickly as possible. The approximately 5 minute exposure to the air resulted in the growth of a black film (which is presumably lithium nitride) on the normally shiny metallic lithium surface. All of the lithium films used in the helium adsorption studies were ablated in hard vacuum at low temperature with the cell near 4 K. First the lithium target was cleaned using the laser to remove the small

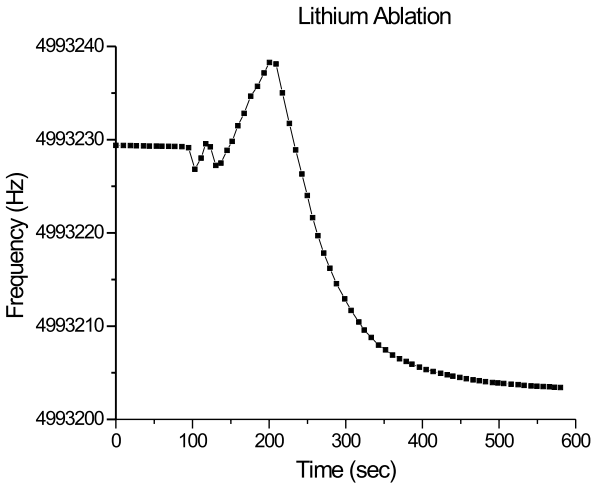


**Fig. 2** The frequency of the QCM as a function of time during PLD of lithium. The QCM was rotated into position for deposition at $t = 120$. The initial frequency rise is due to heating. The frequency subsequently drops as the QCM reaches thermal steady state and the mass increases due to deposition. The QCM was rotated out of position at $t = 300$. The total frequency shift of 26 Hz corresponds to 86.6 layers of lithium

amount of reacted lithium from its surface. During this process, the QCM was rotated so that no material was deposited. The computer controlled mirror was used to raster the beam across a 1 cm square, which was repeated a few times until the shiny surface of the pristine lithium was recovered. The laser parameters were adjusted to the optimal values determined from the room temperature experiments (power level = 61 mJ/pulse, repetition rate = 30 Hz), and while the mirror rastered over the target, the QCM was then rotated so that one side faced the lithium. During the deposition process the QCM resonant frequency was monitored. The QCM was an AT cut 3rd harmonic crystal with a fundamental frequency of 5 MHz and a $5 \times 10^5$ quality factor. One statistical layer of lithium at the bulk density decreased the resonant frequency by 0.3 Hz. The QCM frequency is also temperature dependent, and increases by approximately 3 Hz/K in the temperature range 5–20 K. As the QCM is initially rotated into position, the heating effects of the plasma ball and scattered laser light overwhelm the mass increase due to deposition, so the frequency goes up for several seconds until the QCM reaches a thermal steady state, after which the frequency drops due to mass increase of deposition; this is illustrated in Fig. 2, the deposition rate was 0.5 layers/second. The initial temperature rise of the QCM, which has only a weak thermal link to the rest of the cell, is approximately 15 K despite the fact that the temperature of the cell itself rises by less than 1 K during the deposition. Once the required coverage was reached (typically about 100 layers), the QCM was rotated into the neutral position and then into position to deposit lithium on the other side. Several attempts at annealing were made by raising the lithium substrate temperature to various levels ranging from 20 K to 300 K and durations ranging from 5 minutes to 3 hours. Either no change in the isotherms were observed or the film was converted to a strong binding substrate.

## 3 Isotherms

Isotherms were performed in the cell after the ablation was completed. The cell was then cooled to the operating temperature using the $^4$He evaporative fridge mounted on

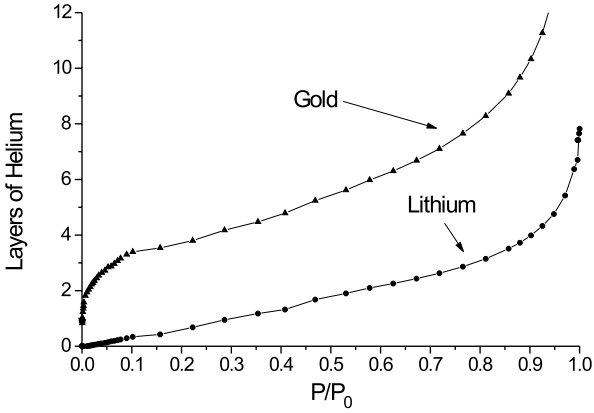


**Fig. 3** Helium coverage as a function of reduced pressure $P/P_o$ at T = 2.45 K. The gold substrate shows a rapid rise in coverage near $P/P_o = 0$, which is due to the solid-like layers characteristic of strong substrates. The lithium substrate shows no strong binding near $P/P_o = 0$ and a nearly linear variation of coverage with reduced pressure until $P/P_o = 0.8$. Near $P/P_o = 1$ the coverage on both substrates diverges, indicating that both are wet at coexistence

top of the cell and thermostatted using a temperature controller. Gas doses were admitted through a capillary and the equilibrium pressure was measured using a room temperature pressure gauge. The cell was equipped with two QCMs; one had gold electrodes as provided by the supplier, and served as a reference strong binding substrate, and the other had the PLD lithium films deposited on top of its gold electrodes. Both the frequency shift $\Delta f$ and the dissipation as measured by the effective resistance $R$ of the equivalent LCR circuit were monitored as a function of pressure using a network analyzer, as described in reference [23]. As gas is added to the cell, the measured frequency shift $\Delta f$ changes because of the added mass of the viscously clamped adsorbed fluid, $\Delta f_{film}$, but also because of viscous interactions with the surrounding vapor and because the elastic properties of quartz are pressure dependent. These effects are described by [23]:

$$\Delta f = \Delta f_{film} - \frac{2 f_o \sqrt{\eta_{vapor}\rho_{vapor}}}{N\pi R_q} + \alpha f_o P \tag{1}$$

where the second term describes viscous coupling to the vapor and the last term is the compression term. $N = 3$ is the harmonic of the QCM, $\eta_{vapor}$ is the viscosity of the helium vapor, $f_o = 5$ MHz is the fundamental frequency of the crystal, $\rho_{vapor}$ is the density of the helium vapor, $\alpha = (1.43693 - 0.00115T) \times 10^{-11}$ is a compression constant, $P$ is the gas pressure in Pa, and $R_q = 8.896 \times 10^6 \frac{\text{kg}}{\text{m}^2\,\text{s}}$ is the acoustic impedance of quartz. The term of primary interest is the first term which is written as [23]

$$\Delta f_{film} = -\frac{4 f_o^2 \sigma_{He}}{N R_q} \tag{2}$$

where $\sigma_{He}$ is the mass per unit area of the helium film. The measured values of $\Delta f$ were corrected for the effects described in (1) and converted into an equivalent coverage in layers, assuming $\sigma_{layer} = 5.208 \times 10^{-8}$ kg/m$^2$.

Figure 3 compares the helium coverage as a function of reduced pressure $P/P_o$ for gold and lithium substrates above the lambda point at T = 2.45 K, so the helium is always in the normal state. The lithium substrate was formed by a two step deposition

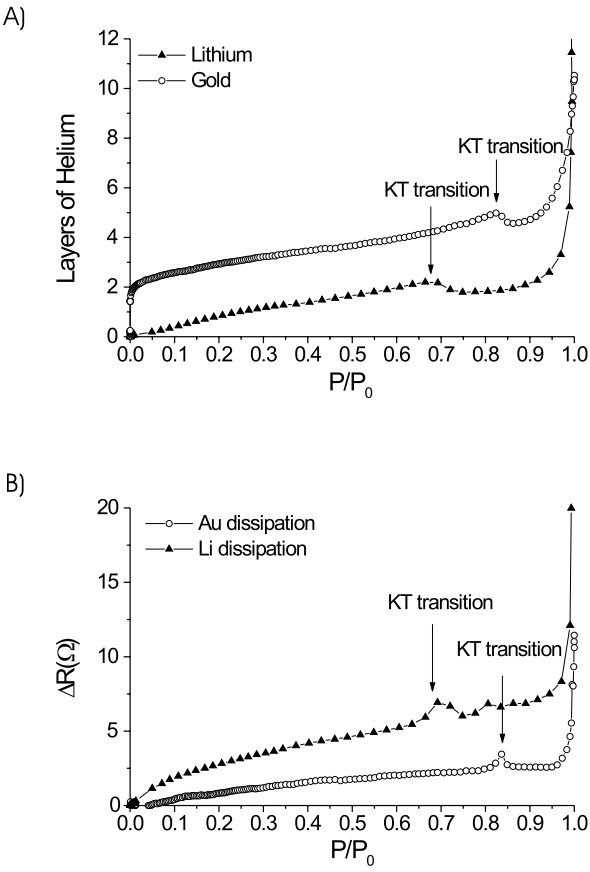


**Fig. 4** Helium isotherms as a function of reduced pressure $P/P_o$ at 1.75 K. (**A**) shows the coverage of helium for both the lithium surface and gold surface. (**B**) shows the dissipation, in units of Ω for the lithium and gold surfaces. The positions of the superfluid transitions are marked with *arrows*. Once again no solid-like layers of helium are observed. The film thickness of the liquid helium at the superfluid transition was the same for gold and lithium, but the transition occurs at a lower reduced pressure on lithium than gold

and has a total thickness of 220 layers. Approximately two layers of helium form on the gold substrate at pressures indistinguishable from zero in our apparatus; these are the solid-like layers characteristic of any strong binding substrate. The helium coverage on the lithium substrate, in contrast, varies continuously and approximately linearly with pressure from $P/P_o = 0$ to $P/P_o = 0.8$. At higher values of $P/P_o$, the coverage on both the lithium and the gold substrates diverges, indicating that both are wet by helium. Note that the coverage on lithium is always less than the coverage on gold, as expected for a weaker substrate.

Figure 4 shows a similar comparison between adsorption isotherms on gold and lithium at T = 1.754 K. At this temperature, the helium films undergo a KT superfluid transition which is marked by a drop in the measured coverage corresponding approximately to the superfluid areal density which is no longer viscously coupled to the substrate. The helium film on the lithium substrate becomes superfluid at a lower value of $P/P_o$ than the film on gold, but the total liquid coverage at the transition is approximately the same value of 2.0 layers on both substrates, assuming that 2.5 layers on gold are solid-like.

The lack of solid like layers of helium and the linear dependence of coverage on pressure allows for a direct measurement of the binding energy of helium to lithium.

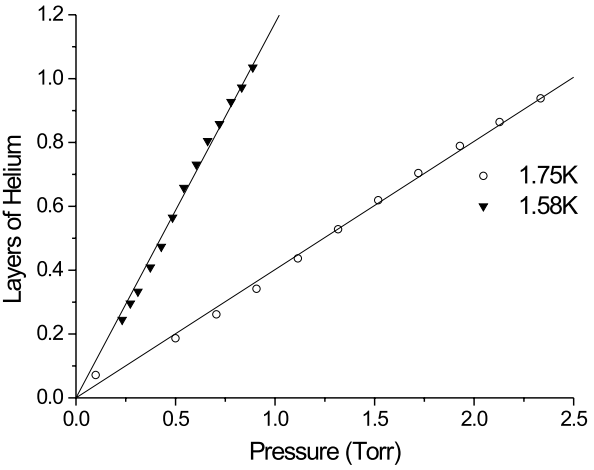


**Fig. 5** The coverage as a function of pressure is shown for coverages under 1 layer for 1.75 K and 1.58 K. The *solid lines* are best fits to the data. The slopes are used to calculate the binding energy of helium on lithium

Assuming that the liquid on the lithium is a 2D Bose gas which is in equilibrium with a 3D ideal gas, the equation for the helium surface density is

$$\sigma = -\frac{M_{He}}{\lambda^2} \ln\left(1 - \frac{P\lambda^3}{kT} \exp\left(\frac{\epsilon}{T}\right)\right) \tag{3}$$

where $\epsilon$ is the binding energy, and $\lambda$ is the de Broglie wavelength. Since at low $P$ the 3D gas is far from the quantum limit, the second term in the argument of the logarithm in (3) is much smaller than 1. When the logarithm is expanded, (3) becomes

$$\sigma = P\frac{M_{He}\lambda}{kT} \exp\left(\frac{\epsilon}{T}\right) \tag{4}$$

which is linear in $P$. The binding energy, $\epsilon$, can be related to experimental observables by solving 2 for $\sigma$ and comparing to 4. This analysis shows that the slope of the low coverage part of the isotherm should be proportional to $\exp(\varepsilon/T)$. Figure 5 shows that the low coverage portion of the isotherms is approximately linear in $P$, and that the slope depends strongly on $T$. This analysis was used to determine the binding energy as a function of temperature, as shown in Fig. 6. The average binding energy of the helium atoms in this temperature range was found to be $-13.69 \pm 1$ K, which is close to the values obtained by Boninsegni and Szybisz [3] for $T = 0.5$. This can be compared to the experimentally determined binding energy of helium on hydrogen preplated substrates, which can be as high as $-22$ K [24].

The adsorption data reported above were obtained on lithium substrates made in a two step process in which approximately 100 layers of lithium was deposited in each step. Thinner lithium substrates fabricated in a single step had peculiar, nonreproducible properties. A typical example of the isotherms we observed on these thinner substrates is shown in Fig. 7. The coverage increases faster than linear in the reduced pressure at low coverage. Two independent KT superfluid transitions are observed, both of which occurred at a lower value of $P/P_o$ than on gold. Both transitions have

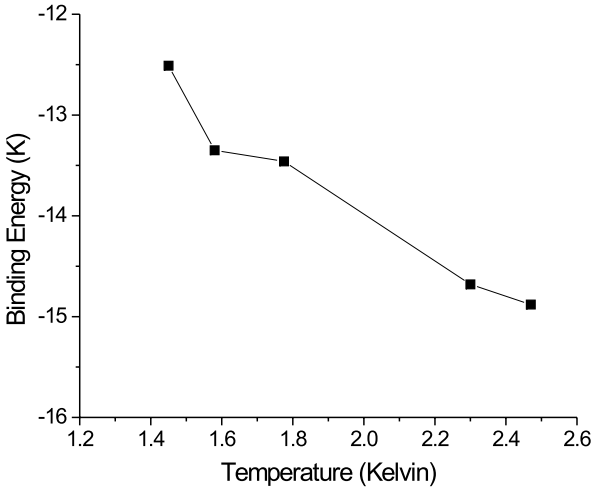


**Fig. 6** The binding energy of helium on lithium, as determined by slopes in Fig. 5, as a function of temperature

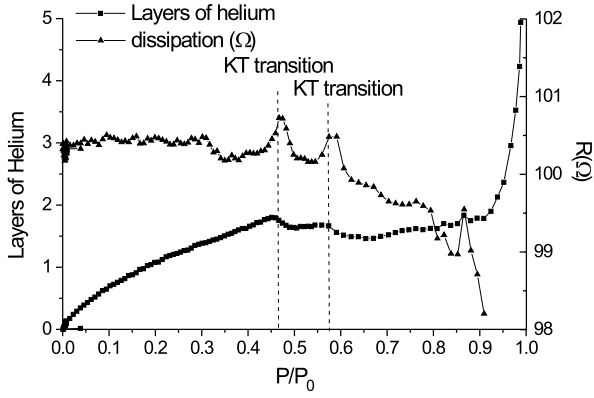


**Fig. 7** A 1.58 K isotherm, which is typical of lithium after the first film was produced. The *triangles* represent the dissipation measured in Ω, the *axis* is on the *right*. The coverage is represented by *solid squares* with the *axis* on the *left*. Two superfluid transition can easily be identified. Each superfluid transition occurs at a lower $P/P_o$ than it would on gold

the conventional characteristic features of mass decoupling and a peak in the dissipation. These qualitative properties were obtained for lithium films prepared with a factor of three variation in both the deposition rates and the final lithium thickness, but the exact values of the reduced pressure at which the superfluid transitions occurred varied from film to film. We also tried to anneal the films in vacuum according to several different protocols up to T = 300 K, but this did not affect the location of the transitions. Experiments in which lithium was deposited on only one side of the QCM showed a single transition, so we believe that the two transitions we observe are due to subtle differences in the properties of the lithium deposited on each side of the QCM. Two factors that might contribute to variations in the lithium films include the kinetics of wetting of lithium on gold and that lithium has two crystallographic phases which are metastable at low temperatures [25–28]. Despite this variability seen in thinner films formed by a single deposition, a second ablation of lithium onto the QCM would produce isotherms which had only one superfluid transition at a repeatable value $P/P_o$ as shown in Fig. 4.

## 4 Conclusion

We have demonstrated that pulsed laser deposition is an effective method for depositing clean metal substrates at low temperature. PLD is a flexible technique that can be used to deposit films of virtually any material. We have used PLD to form lithium substrates and report the first helium adsorption measurements on this surface. Theoretical work has identified lithium as an interesting substrate that should be strong enough to suppress wetting and layering transitions, but not strong enough to form immobile solid-like layers. Our results are in qualitative agreement with these predictions. In the temperature range we investigated, 1.4–2.4 K, the helium coverage on lithium is a smooth and remarkably linear function of pressure, even when the coverage reaches several layers. An analysis of the slopes of the isotherms yields an effective binding energy which is within 20% of the predictions at $T = 0.5$ K. Superfluidity on these substrates has the conventional KT features and occurs at the same liquid helium coverage as on gold if we assume the existence of 2.5 solid-like layers on gold and no solid-like layers on lithium. Superfluid onset occurs at a lower value of the chemical potential on lithium than it does on gold or other strong substrates. This implies that the superfluid phase can be localized by a lithium substrate and that an unusual superfluid-normal boundary exists in the helium film near the edge of a lithium substrate. Below approximately 0.75 K, the first layer of helium is expected to have a liquid-vapor transition [24, 29, 30], which should appear as a discontinuity in an adsorption isotherm. Our experiments so far have been considerably above this temperature, so it is not surprising that we see no evidence of this phenomenon. We hope to extend our measurements into this low temperature regime in the near future.

## References


1. E. Cheng, G. Ihm, M.W. Cole, State of the $^4$He film at monolayer completion. J. Low Temp. Phys. **14**, 519 (1989)
2. M. Boninsegni, M.W. Cole, F. Toigo, Helium adsorption on a lithium substrate. Phys. Rev. Lett. **83**, 2002 (1999)
3. M. Boninsegni, L. Szybisz, Structure and energetics of helium films on alkali substrates. Phys. Rev. B **70**, 024512 (2004)
4. E. Cheng, M.W. Cole, W.F. Saam, J. Treiner, Phase transitions in multilayer helium films. Phys. Rev. B **46**, 967 (1992)
5. A. Chizmeshya, M.W. Chole, E. Zaremba, Weak binding potentials and wetting transitions. J. Low Temp. Phys. **110**, 677 (1998)
6. P.J. Shirron, J.M. Mochel, Atomically thin superfluid helium films on solid hydrogen. Phys. Rev. Lett. **67**, 1118 (1991)
7. P.W. Adams, V. Pant, Superfluid transition in $^4$He films on hydrogen and its effects on the film-vapor coupling. Phys. Rev. Lett. **68**, 2350 (1992)
8. G.A. Csathy, J.D. Reppy, M.H.W. Chan, Substrate-tuned boson localization in superfluid $^4$He films. Phys. Rev. Lett. **91**, 235301 (2003)
9. D. Tulimieri, N. Mulders, M.H.W. Chan, Torsional oscillator study of thin helium films on hydrogen substrates. J. Low Temp. Phys. **119**, 609 (1998)
10. E. Cheng, M.W. Cole, W.F. Saam, J. Treiner, Helium prewetting and nonwetting on weak-binding substrates. Phys. Rev. Lett. **67**, 1007 (1991)
11. J.E. Rutledge, P. Taborek, Prewetting phase diagram of $^4$He on cesium. Phys. Rev. Lett. **69**, 937 (1992)
12. J.E. Rutledge, P. Taborek, Novel wetting behavior of $^4$He on cesium. Phys. Rev. Lett. **68**, 2184 (1992)

13. J.A. Phillips, P. Taborek, J.E. Rutledge, Experimental survey of wetting and superfluid onset of $^4$He on alkali metal surfaces. J. Low Temp. Phys. **113**, 829 (1998)
14. J.A. Phillips, D. Ross, P. Taborek, J.E. Rutledge, Superfluid onset and prewetting of $^4$He on rubidium. Phys. Rev. B **58**, 3361 (1998)
15. J. Kleir, A.F.G. Wyatt, Nonwetting of liquid $^4$He on Rb. Phys. Rev. B **65**, 212504 (2002)
16. L. Szybisz, Wetting of planer substrates of rubidium by liquid films of $^4$He. Phys. Rev. B **62**, 12381 (2000)
17. L. Szybisz, Adsorption of superfluid $^4$He films on player heavy-alkali metals studied with the Orsay-Trento density functional. Phys. Rev. B **67**, 132505 (2003)
18. G. Mistura, H.C. Lee, M.H.W. Chan, Hydrogen adsorption on alkali metal surfaces: Wetting, prewetting and triple-point wetting. J. Low Temp. Phys. **96**, 221 (1994)
19. S.K. So, H.H. Fong, C.F. Yeung, N.H. Cheung, Transmittance and resistivity of semicontinuous copper films prepared by pulsed-laser deposition. Appl. Phys. Lett. **77**, 1099 (2000)
20. J.M. Warrender, M.J. Aziz, Evolution of Ag nanocrystal films grown by pulsed laser deposition. Appl. Phys. A **79**, 713 (2004)
21. V. Apaja, E. Krotscheck, M.D. Miller, The phase of submonolayer $^4$He films near monolayer completion. J. Low Temp. Phys. **145**, 369 (2006)
22. T. McMillan, J.E. Rutledge, P. Taborek, Ellipsometry of liquid helium films on gold, cesium, and graphite. J. Low Temp. Phys. **138**, 995 (2005)
23. R.J. Lazarowich, P. Taborek, Superfluid transitions and capillary condensation in porous media. Phys. Rev. B **74**, 024512 (2006)
24. P.S. Ebey, O.E. Vilches, Determination of the thermodynamic phases of $^4$He adsorbed on $H_2$ plated graphite. J. Low Temp. Phys. **101**, 469 (1995)
25. C.S. Barrett, X-ray study of the alkaline metals at low temperatures. Acta Cryst. **9**, 671 (1956)
26. O. Blaschko, V. Dmitriev, G. Krexner, P. Toledano, Theory of the martensitic phase transformation in lithium and sodium. Phys. Rev. B **59**, 9095 (1999)
27. A.W. Overhauser, Crystal structure of lithium at 4.2 K. Phys. Rev. Lett. **53**, 64 (1984)
28. W. Schwarz, O. Blaschko, bcc instability of lithium at low temperatures. Phys. Rev. B **44**, 6785 (1991)
29. M.C. Gordillo, D.M. Ceperley, Path-integral calculation of the two-dimensional $^4$He phase diagram. Phys. Rev. B **58**, 6447 (1998)
30. J. Nyeki, R. Ray, G. Sheshin, V. Maidanov, V. Mikheev, B. Cowan, J. Saunders, Structure and superfluidity of $^4$He films on plated graphite. Low Temp. Phys. **23**, 379 (1997)